Atmos. Chem. Phys. Discuss., 11, 30091–30124, 2011
www.atmos-chem-phys-discuss.net/11/30091/2011/
doi:10.5194/acpd-11-30091-2011

Atmospheric Chemistry and Physics Discussions

Uptake coefficient of H_2O_2 on ice

H. Yan and L. T. Chu

Wadsworth Center, NYS Health Department, and Department of Environmental Health Sciences, State University of New York, Albany, NY 12201-0509, USA

Received: 20 October 2011 – Accepted: 24 October 2011 – Published: 8 November 2011

Correspondence to: L. T. Chu (lchu@albany.edu)

Published by Copernicus Publications on behalf of the European Geosciences Union.

Abstract

H_2O_2 uptake coefficients on ice surfaces, over a temperature range from 190 to 220 K, have been studied in a flow reactor coupled with a differentially pumped quadrupole mass spectrometer. The initial uptake coefficient increases with an increase in H_2O_2 pressure and a decrease in temperature. The results were analyzed using surface kinetics, and the analysis shows that the uptake involves both H_2O_2 adsorption and surface aggregation. H_2O_2 desorption kinetics supports lateral attractive interactions among adsorbed H_2O_2 on ice. The result can be used to model the heterogeneous H_2O_2 loss on snow/ice surfaces and cirrus clouds as a function of the H_2O_2 concentration and temperature.

1 Introduction

Hydrogen peroxide (H_2O_2) is found both in air and in condensed phases such as clouds and aerosols, as well as on the ground-level snow and icepacks at higher latitudes, with the deposition of H_2O_2 from the atmosphere as a major source (Sigg and Neftel, 1991; Bales et al., 1995; Hutterli et al., 2001; Vione et al., 2003; Seinfeld and Pandis, 2006). Field measurements have shown that snow/ice has large capacity to take up H_2O_2 (Bales et al., 1995). H_2O_2 is known to be a source of OH radicals, produced photochemically from Reaction (R1) in/on the icepack and cirrus cloud ice (Chu and Anastasio, 2005; Jacobi et al., 2006; France et al., 2007).

$$H_2O_2(\text{ad}) + h\nu \rightarrow 2\text{OH} \qquad \text{(R1)}$$

The photochemically produced OH radicals alter the OH concentration and oxidative capacity in/on the icepack, cirrus clouds and the atmosphere above ice interfaces. This changes the lifetimes of atmospheric species, such as organics and halogens, and affects tropospheric chemistry. The rate of H_2O_2 taken up on ice surfaces can affect the amount of H_2O_2 on ice surfaces so as to affect the subsequent H_2O_2 photolysis

ACPD
11, 30091–30124, 2011

product yield in Reaction (R1). Recent studies show the reactivity of photochemically produced OH toward aromatics bimolecular reactions at the air-ice interface is significantly suppressed relative to that in veins and packets within bulk ice (Kahan et al., 2010). The poor OH partition on ice surfaces and the recombination of OH to H_2O_2 are suggested to be a cause. A better understanding of H_2O_2-ice surface interactions is necessary to shed light on the nature of OH and H_2O_2 on the ice surface. In addition, heterogeneous reaction of H_2O_2 with bromide on the icepack is suggested to activate bromide to photochemically active halogens (Grannas et al., 2007). This pathway may alter the partitioning of halogen species and affect the distribution of ozone. To assess the significance of the heterogeneous reaction of H_2O_2 with bromide on ice surfaces and to fully understand the nature of H_2O_2-ice surface photochemistry, one needs to know the rate of H_2O_2 taken up on ice surfaces and adsorption of H_2O_2 on ice. Thus, it is necessary to gain the knowledge of the uptake coefficient of H_2O_2 on ice surfaces, to reveal the nature of H_2O_2-ice surface photochemistry and mechanism of H_2O_2 reaction with bromide on ice surfaces.

Currently, studies are mainly concentrated on the amount of H_2O_2 taken up by ice surfaces and interactions between ice and H_2O_2. Clegg and Abbatt (2001) have determined that the uptake amount of H_2O_2 on ice surfaces increases with an increase in $[H_2O_2]$. Pouvesle et al. (2010) showed that uptake amount of H_2O_2 on ice surfaces increases with an increase in $[H_2O_2]$ and a decrease in temperature from 233 to 203 K. However, studies of the rate of H_2O_2, uptake coefficient, taken up by ice surfaces are infrequent. Conklin et al. (1993) showed that the proportion of H_2O_2 taken up by ice at low temperatures is higher than that at higher temperatures (from 228 to 270 K). A sticking coefficient was estimated to be on the order of 0.02, from the advection-dispersion model (Conklin et al., 1993). To the best of our knowledge, no study in literature has reported a value for uptake coefficient of H_2O_2 on ice at temperatures lower than 228 K, a temperature range found in the upper troposphere and polar region. The effects of temperature and H_2O_2 partial pressure on the uptake coefficient at low temperature are unknown. Thus, the objective of this study is to determine H_2O_2 uptake coefficient

ACPD
11, 30091–30124, 2011

at low temperature.

In this paper, we report the H_2O_2 uptake coefficient as a function of temperature and pressure, and shed light on the nature of H_2O_2 interaction with ice surfaces. In the following sections, we briefly describe the experimental procedures, and then present our results for the initial uptake coefficient of H_2O_2 on ice surfaces. Following a discussion of our findings, we compare our results with literature values, and present the implications of this study for atmospheric chemistry.

2 Experimental

The uptake coefficient, γ, is defined as the ratio of the number of H_2O_2 molecules that are taken up by the ice surface to the total number of H_2O_2 molecules colliding with that surface. γ was determined when an ice film was freshly prepared and the ice surface was clean; thus, it is termed the initial uptake coefficient, γ_w. The determinations of γ_w were performed in a flow reactor coupled with a differentially pumped quadrupole mass spectrometer, QMS (Extrel; C50 Electronics). The details of the apparatus have been described in our previous publications (Chu and Heron, 1995; Chu and Chu, 1999; Yan et al., 2009). A brief summarization, noting modifications of the apparatus that were used in the present work, follows.

2.1 Flow reactor

The double-jacketed cylindrical flow reactor (35 cm in length, with 1.7 cm inner diameter) was made of Pyrex glass. The outer jacket was a vacuum layer to maintain the temperature of the reactor. Temperature of the reactor was regulated by a liquid-nitrogen-cooled methanol circulator (Neslab) and was measured with a pair of J-type thermocouples located in the middle and at the downstream end of the reactor. The experimental temperature was reported as the average from the two thermocouple readings. During the experiment, temperature was maintained within the range of 190

ACPD
11, 30091–30124, 2011

to 220 K; the stability of temperature was better than ± 0.2 K. Pressure inside the reactor was controlled by a downstream throttle valve (MKS Instruments; Model 653B), and was measured with a high-precision Baratron pressure gauge (MKS Instruments; Model 690A). The typical total pressure used was 0.270 Torr. The stability of the pressure was better than 0.001 Torr in the experiments. A double-capillary movable injector was used to admit gaseous H_2O_2 and H_2O vapor into the flow reactor individually, for determinations of the initial uptake coefficient. The injector was sealed to the reactor by O-rings. Room-temperature dry air was passed through the outside of the capillary, to keep it warm so as to prevent condensation of the water vapor and H_2O_2 on the capillary wall.

2.2 Ice film preparation

High-purity deionized water (> 18 MΩ cm, Barnstead; Model D11931) was degassed by a passage of helium carrier gas (Matheson; 99.9995 %) through the reservoir, which was maintained at 293.2 ± 0.1 K by a refrigerated circulator (Neslab; Model RTE-100LP), to remove dissolved gases in water. Helium saturated with the water vapor was introduced to the reactor, maintained at a temperature of the experiment, through an inlet of the double-capillary injector. The injector was then pulled out at a slow, constant speed, to allow a uniform ice film to form on the inner wall of the reactor. The amount of ice deposited was determined from the mass flow rate of the H_2O-He mixture (as measured by a Hasting mass flow meter), the H_2O-He mixing ratio, and the deposition time. The average film thickness, h, was calculated from the mass of ice, the geometric area of the ice film on the flow reactor, and the bulk density ($\rho_b = 0.63\,g\,cm^{-3}$) of vapor-deposited ice (Keyser and Leu, 1993a). The effect of the ice-film volatile nature on the film thickness is negligible because of the short experimental time scale (minutes) to measure γ_w.

ACPD
11, 30091–30124, 2011

2.3 H_2O_2 preparation and calibration

Highly concentrated H_2O_2 solution (93 ± 1 wt %) was prepared by vacuum distillation of a 50 wt % H_2O_2 (Sigma-Aldrich) solution (Maass and Hatcher, 1920). A 98 wt % H_2SO_4 trap was used during the vacuum distillation, to assist in the removal of H_2O and to overcome a eutectic point (61.2 wt % and 217.1 K; Giguère and Masee, 1940; Schumb et al., 1955). Teflon tubing and connectors were used in the distillation system to avoid potential wall-catalyzed H_2O_2 decomposition. The temperature of the H_2O_2 solution was controlled with the use of a water-bath varying from 278 to 293 K during the distillation. The pressure in the distillation system was controlled by a needle valve. The concentrated H_2O_2 solution was kept in dark at 265.3 K, since low temperature reduces the propensity for H_2O_2 decomposition.

Determination of the H_2O_2 concentration in the gas and aqueous phase of the prepared solution entailed two steps. First, $[H_2O_2]$ in solution was determined to be 93 ± 1 wt % from the measurements of the refractive index at 293.2 K (Giguère and Geoffrion, 1949), using a refractometer (Bausch & Lomb; Model 33.46.10). The density of the H_2O_2 solution was determined to confirm the $[H_2O_2]$ in solution (Huckaba and Keyes, 1948). Second, using (i) the vapor-liquid equilibrium data of 93 wt % H_2O_2 at 273.2 K and 283.2 K (Scatchard et al., 1952; Schumb et al., 1955); and (ii) the QMS signals of the H_2O_2 vapor above the solution, determined at 265.3, 273.2 and 283.2 K, the gaseous $[H_2O_2]$ of the 93 wt % H_2O_2 solution was determined, from a linear plot of the H_2O_2 QMS signals versus the gaseous H_2O_2 concentration, to be 0.106 ± 0.02 Torr at 265.3 K. However, taking the uncertainties of H_2O_2 vapor-liquid data (Manatt and Manatt, 2004) and the measurements into consideration, the accuracy of the gaseous $[H_2O_2]$ was estimated to be ± 30 %.

The H_2O_2-He mixture was prepared by bubbling helium through the 93 wt % H_2O_2 solution in a glass bubbler at 265.3 K. The total pressure in the bubbler was measured by a Baratron pressure gauge (MKS Instruments; Model 722A). The typical H_2O_2-to-He mixing ratio was 10^{-4} to 10^{-5}. The flow rate of the H_2O_2-He mixture was controlled

ACPD
11, 30091–30124, 2011

by a metering valve. The H_2O_2-He mixture, along with additional helium carrier gas, was admitted to the flow reactor via PFA tubing. The tubing was passivated by the H_2O_2-He mixture, to enable equilibrium to be established, as monitored by the QMS prior to every measurement.

2.4 Determination of initial uptake coefficient

The initial uptake coefficient, γ_w, of H_2O_2 on ice was determined as follows. First, a fresh ice film ($\sim$ 20 cm in length) was prepared by water-vapor deposition on the inner wall of the flow reactor for each determination. The background QMS signal at $m/z = 34$ was recorded. Second, the H_2O_2-He mixture was admitted to the other inlet of the double capillary injector. Before H_2O_2 molecules came in contact with the ice surface, the initial H_2O_2 signal, $[H_2O_2]_i$, was measured by the QMS. After the $[H_2O_2]_i$ stabilized, the sliding injector was pulled out toward the upstream end of the flow reactor, 1 cm at a time. The loss of H_2O_2 was monitored at $m/z = 34$ by the QMS as a function of the injector distance z. Figure 1 shows a typical plot of the QMS signal for the H_2O_2 loss on an ice-film surface. The initial H_2O_2 signals were determined under the conditions both with and without the ice film in the reactor, and the difference in H_2O_2 signals was subtracted for the plot. For the first-order loss rate under laminar flow conditions, the following equation holds for H_2O_2:

$$\ln[H_2O_2]_z = -k_s(z/v) + \ln[H_2O_2]_0 \quad (1)$$

where z is the injector position, v is the average flow velocity, z/v is the duration of contact (time) of H_2O_2 with the ice surface, $[H_2O_2]_z$ is the gaseous H_2O_2 concentration measured by the QMS at position z, and the subscript 0 is the initial injector reference position. The first-order loss rate constant (k_s) was determined to be $444 \pm 13\,s^{-1}$, from the slope of the least-squares fit to the experimental data (Fig. 1). The k_s value was corrected for gas-phase radial diffusion using a method outlined by Brown (1978), and the corrected rate constant was termed k_w. This correction worked well for our long and thin flow reactor (Davis, 2008). A diffusion coefficient for H_2O_2 in helium was used

ACPD
11, 30091–30124, 2011

for the gas-phase diffusion correction; it was calculated, from the Chapman-Enskog equation (Cussler, 1984), to be 698 $cm^2\,s^{-1}$ at 0.270 Torr and 190 K. Assuming that there is no other major gas-phase H_2O_2 loss besides the heterogeneous loss on ice, then the observed gas-phase H_2O_2 loss rate is equal to the heterogeneous loss rate. Figure 1 shows that there is no measurable H_2O_2 loss on the cold Pyrex wall surface and ensures that the assumption is valid.

The initial uptake coefficient can be calculated from k_w as follows, using the geometric area of the flow reactor (Motz and Wise, 1960; Keyser et al., 1991; Chu and Chu, 1999):

$$\gamma_w = \frac{2rk_w}{\omega + rk_w} \tag{2}$$

where ω is the mean molecular velocity, and r (0.85 cm) is the radius of the flow reactor.

It is generally accepted that a vapor-deposited ice film has internal surface areas and is porous (Keyser and Leu, 1993a,b). In order to obtain a "true" uptake coefficient γ_t, assuming the film is a geometrically smooth surface, we have corrected γ_w for contributions from the internal surface areas. On the basis of findings from previous studies conducted at similar conditions (Keyser et al., 1991, 1993; Keyser and Leu, 1993a), H_2O-ice films can be approximated as stacked layers of hexagonally close-packed spherical granules, and cylindrical pores are assumed. The true uptake coefficient, γ_t, is related to γ_w by Keyser et al. (1993):

$$\gamma_t = \frac{\sqrt{3}\gamma_w}{\pi\{1+\eta[2(N_L-1)+(3/2)^{1/2}]\}} \tag{3}$$

where the effectiveness factor, $\eta = \varphi^{-1}\tanh\varphi$, is the fraction of the film surface that participates in the reaction, $\varphi = \left((N_L-1)\left(\frac{2}{3}\right)^{1/2}+\left(\frac{1}{2}\right)\right)\left[\frac{3\rho_b}{2(\rho_t-\rho_b)}\right](3\tau\gamma_t)^{1/2}$, ρ_t (0.925 $g\,cm^{-3}$) and ρ_b are true density and bulk density of the ice, τ is the tortuosity factor, and N_L is the number of granule layers (Chu et al., 1993; Keyser et al., 1993).

ACPD
11, 30091–30124, 2011

Detailed calculations can be found in Keyser et al. (1991, 1993). $\tau = 3.3$ (see Sect. 3.1) was used in the above calculation. This value is within the typical recommended range of 2 to 6 for porous solids (Satterfield, 1970). The true uptake coefficient was subsequently determined to be $\gamma_t = 3.9 \times 10^{-3}$ (Fig. 1).

2.5 H_2O_2 QMS signal

As shown below, the measured QMS signal at $m/z = 34$ was indeed from H_2O_2 molecules. We have determined that QMS signal ratio of $m/z = 34$ to $m/z = 32$ was $(6 \pm 2) \times 10^{-3}$ and 0.15 ± 0.05, before and after admitting H_2O_2 (4×10^{-5} Torr) to the flow reactor, respectively. The value, $(6 \pm 2) \times 10^{-3}$, was close to the expected signal ratio of 4×10^{-3} for $^{34}O_2 : {}^{32}O_2$, calculated from the natural abundance of $^{18}O : {}^{16}O$ (0.2 : 100) (Lide, 2008). 0.15 ± 0.05 was approximately 25-fold higher than $(6 \pm 2) \times 10^{-3}$, suggesting that the $m/z = 34$ signal was from H_2O_2 rather than $^{18}O^{16}O$. In addition, the contribution of $^{34}O_2$ to the $m/z = 34$ signal was determined to be $< 2.7\,\%$ of the total $m/z = 34$ signal. k_s was calculated from the difference in logarithm signals (cf. Eq. (1)), and we found that the k_s value increased approximately 3.5 %, after taking the $^{34}O_2$ signal correction into consideration. The correction is smaller than the experimental uncertainty. In order to reduce the data acquisition time, we did not measure $m/z = 34$ and $m/z = 32$ signals simultaneously in all experiments, but we did correct the measured k_s value by 3.5 % for the results in Tables 1 and 2.

We observed that the measured initial H_2O_2 signal, with the ice deposited in the reactor, was higher than that without the ice film, suggesting that the H_2O_2 signals were affected by the presence of the ice film. The H_2O_2 signal enhancement is not due to the interference of H_2O signal since H_2O has no $m/z = 34$ fragment. Furthermore, we found that the H_2O_2 signal increased with an increase in the H_2O vapor pressure. The nature of this $m/z = 34$ signal enhancement by the H_2O vapor pressure is not clear to us, however, it is possible that this observation was due to the formation of $H_2O_2 \cdot (H_2O)_n$ clusters (Kulkarni et al., 2006) in the ionization region, and altered the

ACPD
11, 30091–30124, 2011

H_2O_2 QMS fragmentation pattern, leading to an enhanced H_2O_2 signal at $m/z = 34$. We have subtracted the enhancement of the initial H_2O_2 signal due to the presence of ice films, from the measured initial $m/z = 34$ signals. However, during the uptake coefficient measurement, when the injector was pulled out, the temperature of ice films varied slightly (1 to 2 K). As a result, this affected the measured H_2O_2 signal slightly. We have constructed a calibration curve of the H_2O_2 QMS signal versus the H_2O vapor pressure, and the H_2O_2 signal changes due to the temperature effect were then corrected.

It was estimated that $< 0.5\,\%$ of the H_2O_2 vapor would be decomposed over the 93 wt % H_2O_2 solution (Manatt and Manatt, 2004). The heterogeneous decomposition rate of H_2O_2 on a Pyrex glass could be ignored since the rate constant was estimated to be 10^{-2}–$10^{-5}\,s^{-1}$ at 220 K (Schumb et al., 1955). Thus, the effect of the H_2O_2 decomposition on measured $[H_2O_2]$ was negligible.

2.6 Temperature programmed desorption

Temperature programmed desorption (TPD) experiments were conducted to investigate the desorption kinetics of H_2O_2 on ice. An ice film was prepared on the inner wall of reactor first, followed by the exposure of the ice surface to gaseous H_2O_2 at 190 K. The surface was then heated with a linear heating rate of $\sim 1.2\,K\,min^{-1}$, up to 283 K. The signals of the desorbed species, H_2O_2 and H_2O, were collected and plotted as a function of temperature. The temperature resolution was approximately 0.5 K.

3 Results

3.1 The effect of ice-film thickness on uptake coefficient

The effect of ice-film thickness on the initial H_2O_2 uptake coefficient was studied to investigate the morphology of the ice film. We varied the ice-film thickness, h, from 1.0 to 51 µm, at 190 K. Figure 2 shows that the initial uptake coefficient, γ_w, of H_2O_2 on

ACPD
11, 30091–30124, 2011

ice surfaces increased rapidly from 8.8×10^{-3} to 1.3×10^{-2} when $h \le 4.0\,\mu m$, but then γ_w remained nearly constant, $(1.3\pm0.1)\times10^{-2}$, for $h > 4.0\,\mu m$. This pattern suggests that the ice film is porous and has internal surface areas. H_2O_2 molecules can gain access to the internal surfaces via pore diffusion. The results were modeled using the hexagonally close-packed spherical granule pore diffusion model (Keyser et al., 1993), Eq. (3). The solid line in Fig. 2 shows the result of nonlinear least-squares fit to the experimental data. Since N_L in Eq. (3) is a function of thickness, an empirical relationship between N_L and h is assumed to be $N_L = a + b\log(h + c)$, where a, b, and c are fitting parameters (Keyser et al., 1993; Jin and Chu, 2007). On the basis of the least-squares fit (γ_w vs. h), we have determined that $\tau = 3.3\pm1.0$ and $N_L = 17$ for a $36.1\pm1.8\,\mu m$ thick ice film, and $N_L = 13$ for a $14.7\pm1.5\,\mu m$ thick ice film. The true uptake coefficient γ_t of H_2O_2 on ice was also determined, from the nonlinear least-squares fit, to be $(1.1\pm0.2)\times10^{-3}$ at 190 K.

3.2 The effect of H_2O_2 concentration on uptake coefficient

The uptake coefficient of H_2O_2 on ice was determined as a function of H_2O_2 partial pressure at 189.9 ± 0.5 K, and the results are shown in Fig. 3. When the H_2O_2 partial pressure was increased from 7.9×10^{-6} to 4.7×10^{-5} Torr, the γ_w value increased from 1.4×10^{-2} to 4.7×10^{-2}; and γ_t increased from 1.3×10^{-3} to 8.8×10^{-3} (Fig. 3 and Table 1). The solid line in Fig. 3 is a fit to the experimental data (see details in Sect. 4.1). The results show that the higher the partial H_2O_2 pressure, the greater the initial uptake coefficient on the ice surface, suggesting that there is attractive interaction among adsorbed H_2O_2 molecules. The detailed experimental conditions are listed in Table 1, and the γ_t values presented in Table 1 were calculated using τ and N_L values from Sect. 3.1. The error bars in Fig. 3 and the errors listed in Table 1 include the systematic errors related to the pressure gauges, digital thermometers, mass flow meters, and the $m/z = 34$ signal corrections, estimated collectively to be approximately 10 %, and 1 standard deviation $\pm\sigma$ of the mean value. Every k_s value listed in Table 1 is

ACPD
11, 30091–30124, 2011

an average of two to five measurements, and each measurement was conducted on a freshly prepared ice film.

3.3 The effect of temperature on uptake coefficient

The values of the initial uptake coefficient were determined at a number of ice-film temperatures. We employed a thicker ice film, 36.1 ± 1.8 µm, to cover the entire temperature range from 190 to 220 K. Table 2 summarizes the results. The initial uptake coefficient for H_2O_2, γ_w, decreased from 1.4×10^{-2} to 2.6×10^{-3}, as temperature of the ice film increased from 190 to 220 K. This trend is clearly consistent with the H_2O_2 heterogeneous loss on ice surfaces. The true uptake coefficient, γ_t, also decreased from 1.2×10^{-3} to 6.6×10^{-5} when temperature increased from 190 to 220 K (Fig. 4). The solid line in Fig. 4 was a fit to the experimental data (see Sect. 4.1).

3.4 Consecutive determinations of γ

Figure 5 shows four repetitions of the determination of an uptake coefficient at 190.0 K. The first measurement was conducted on a freshly prepared ice surface. Once the initial H_2O_2 signal was stable, the injector was pulled out 1 cm at a time toward the upstream end of the flow reactor. γ_w of H_2O_2 on the ice surface was determined to be 1.8×10^{-2}. The injector was then pushed back to the downstream end to enable subsequent measurements to be made on the same ice film. We allowed the H_2O_2 signal to be stabilized for subsequent measurements, and the 2nd, 3rd and 4th determinations of the uptake coefficient were made on the same ice surface. The corresponding uptake coefficients were 1.8×10^{-2}, 1.8×10^{-2} and 1.7×10^{-2}. Within the uncertainty of the measurement (~ 15 %), γ is constant. The results suggest that the adsorption of a small amount of H_2O_2 on the ice surface, in a short uptake time period, does not deactivate the ice surface.

ACPD
11, 30091–30124, 2011

3.5 Temperature programmed desorption

Panel (a) in Fig. 6 depicts a series of TPD profiles of H_2O_2, at various H_2O_2 exposures on ice surfaces. The H_2O_2 exposed ice surface was heated from 190 to 283 K; and since no H_2O_2 signal was found above 260 K, we only present data obtained from 190 to 260 K. Panel (a) shows that as the H_2O_2 exposure time increased from 5, 10, 20, 30 to 45 min at 2.2×10^{-5} Torr (5-min exposure is equivalent to 6600 L), the desorption temperature, T_d, of the first peak of each given desorption profile increased from 201.5, 206.0, 210.5, 213.0 to 216.0 K, correspondingly. This suggests that adsorbed H_2O_2 has lateral attractive interaction to aggregate H_2O_2 together on the surface. Also, TPD profiles suggest there is a considerable amount of H_2O_2 molecularly adsorbed on the surface, since the parent peak of H_2O_2 was detected. However, the T_d for a desorption peak centered at 225.0 K in each desorption profile remained unchanged, 225.0 ± 0.5 K, with an increase in H_2O_2 exposure (Panel (a) in Fig. 6). By varying the ice film thickness, we found that T_d of this desorption peak increased with an increase in ice-film thickness and T_d in each H_2O_2 desorption profile was the same as the ice T_d, i.e., 225.0 K for 14.3 µm ice film and 229.5 K for 36.0 µm ice film (Panel (b) of Fig. 6). The T_d value of the middle desorption peak in each H_2O_2 desorption profile was approximately at 219.0 ± 0.5 K.

4 Discussion

4.1 Uptake coefficient of H_2O_2 on ice

Figure 3 shows that γ_t of H_2O_2 on ice films increases with increasing $P_{H_2O_2}$, and this observation cannot be explained by the precursor model (Masel, 1996), which predicts that γ_t decreases as $P_{H_2O_2}$ increases (see details below). $P_{H_2O_2}$ used in Fig. 3 is higher than the saturation vapor pressure of solid H_2O_2 at 190 K, $\sim1\times10^{-6}$ Torr (Dean, 1999), providing a condition for H_2O_2 to aggregate or associate on the surface, and

ACPD
11, 30091–30124, 2011

the aggregation is also supported by results of TPD. Bowker and King (1979) shows that the sticking coefficient of nitrogen on W(110) increases with increasing nitrogen coverage at 90 and 120 K, and the observation is attributed to the attractive lateral interaction between the adsorbed nitrogen. Aggregation is also used to explain the trend for the sticking coefficient increases with increasing water coverage on Pt{110}-(1×2) (Panczyk et al., 2009). By analogous, we may explain the increase in uptake coefficient with increasing $P_{H_2O_2}$ by considering both adsorption and aggregation of H_2O_2 on ice surfaces. The process is illustrated using the following equations.

$$H_2O_2(g) \underset{k_{-1}}{\overset{k_1}{\rightleftharpoons}} H_2O_2(p) \quad \text{(R2)}$$

$$1-f\ H_2O_2(p) \underset{k_{-2}}{\overset{k_2}{\rightleftharpoons}} H_2O_2(a) \quad \text{(R3)}$$

$$f\ H_2O_2(p) \underset{k_{-3}}{\overset{k_3}{\rightleftharpoons}} 1/n(H_2O_2)_n \quad \text{(R4)}$$

Reaction (R2) represents that gaseous H_2O_2 forms a weakly bounded precursor state, H_2O_2(p), on the surface, and H_2O_2(p) can be either desorbed back to the gas phase, or proceed to an adsorption state H_2O_2(a) (Reaction R3). At the same time, $(H_2O_2)_n$ aggregation is allowed on the surface (Reaction R4). Furthermore, we assume that a small fraction, f, of H_2O_2(p) is aggregated to form islands on the surface, and H_2O_2(g) is only adsorbed on the unoccupied surface.

Experimentally, the net loss of gas-phase H_2O_2 onto the ice-film surface was observed, and can be expressed as:

$$-\frac{d[H_2O_2]}{dt} = k_1 P_{H_2O_2} - k_{-1}[H_2O_2(p)] \quad (4)$$

$[H_2O_2(p)]$ can be solved using the steady-state approximation, $d[H_2O_2(p)]/dt = 0$, and $[H_2O_2(p)] = \frac{k_1 P_{H_2O_2}}{k_{-1}+k_2(1-f)+k_3 f}$, where we assume the reverse rates of Reactions (R3) and (R4) are slow. Since the amount of H_2O_2 adsorbed on the ice surface is

ACPD
11, 30091–30124, 2011

low ($\theta < 0.1$), we assume f is proportional to H_2O_2 surface coverage θ by $f = c\theta$, and θ can be expressed as $\theta \approx bP_{H_2O_2}$, where b is a Langmuir adsorption constant. The uptake coefficient can then be expressed as:

$$\gamma_t = \frac{-\frac{d[H_2O_2]}{dt}}{\frac{P_{H_2O_2}\omega}{4}\frac{S}{V}} = \frac{4Vk_1}{\omega S}\frac{k_2(1-f)+k_3 f}{k_{-1}+k_2(1-f)+k_3 f} \quad (5)$$

where S/V is the surface-to-volume ratio of the flow reactor. Furthermore, when we combine constants together, $a = \frac{4Vk_1}{\omega S}\frac{k_3}{k_{-1}+k_3}$, $m = \frac{4Vk_1}{\omega S}\frac{k_2-k_3}{k_{-1}+k_3}$, $n = \frac{k_2-k_3}{k_{-1}+k_3}$ and $K = bc$, Eq. (5) can be written as:

$$\gamma_t = \frac{a + me^{-KP_{H_2O_2}}}{1 + ne^{-KP_{H_2O_2}}} \quad (6)$$

Equation (6) was used to fit the data of γ_t versus $P_{H_2O_2}$, and the fitted result is shown as a solid line in Fig. 3. The solid line replicates the experimental results very well, suggesting that the uptake of H_2O_2 on ice surfaces is accompanied by both adsorption and aggregation of H_2O_2 on ice surfaces.

If we ignore the aggregation of H_2O_2, i.e., $f = 0$, and assume that Reactions (R2) and (R3) are the only steps to take place on the ice surface, with Reaction (R3) as the rate-determining step, then γ_t can be expressed as:

$$\gamma_t = \frac{-\frac{d[H_2O_2]}{dt}}{\frac{P_{H_2O_2}\omega}{4}\frac{S}{V}} \approx \frac{4V}{\omega S}\frac{k_2 S_o}{\frac{k_{-1}}{k_1} + \frac{k_2}{k_{-2}}P_{H_2O_2}} \quad (7)$$

where S_O is the total surface sites (Masel, 1996). Equation (7) shows that γ_t decreases as $P_{H_2O_2}$ increases. Equation (7) cannot model the observation, and the fitted result is shown as the long dashed line in Fig. 3. This shows that the precursor model cannot predict our results.

ACPD
11, 30091–30124, 2011

On the other hand, if we assume the aggregation (island formation) of H_2O_2 on ice surfaces is the only pathway, i.e., $f = 1$, with Reaction (R4) as the rate-determining step, and then $[H_2O_2(p)] = \frac{k_1 P_{H_2O_2}}{k_{-1}+k_3}$, γ_t can be written as:

$$\gamma_t = \frac{-\frac{d[H_2O_2]}{dt}}{\frac{P_{H_2O_2}\omega}{4}\frac{S}{V}} = a - \frac{b'}{P_{H_2O_2}} \quad (8)$$

where $b' = \frac{4V}{\omega S} k_{-3}[(H_2O_2)_n]^{1/n}$. Assuming $(H_2O_2)_n$ is hydrogen bonded and is stable on the surface and the reverse reaction in Reaction (R4) is slow, and then the $[(H_2O_2)_n]$ is approximately unchanged, so as b'. The result of Eq. (8) is essentially the same as the result from the condensation model (Brown et al., 1996). We used Eq. (8) to fit the data of γ_t versus $P_{H_2O_2}$, and the fitted result is shown as the dotted line in Fig. 3. The dotted line cannot represent the result well. By comparing the results of three processes (Fig. 3), we conclude that the uptake of H_2O_2 on ice is accompanied by both aggregation and adsorption of H_2O_2 on ice surfaces, and this explains the observation $-\gamma_t$ increases with increasing $P_{H_2O_2}$ very well.

Figure 4 shows that γ_t decreases as temperature increases. We attribute the decrease in γ_t to be kinetics. Because the surface area of vapor-deposited ice reduces approximately 2-fold from 200 to 265 K (Keyser and Leu, 1993a), and the decrease in the ice surface area is substantially smaller than the decrease in γ_t from 190 to 220 K (18-fold). The experimental observation can be explained using Eq. (5). The data in Fig. 4 were collected at $P_{H_2O_2} = 8.9 \times 10^{-6}$ Torr, which is lower than the H_2O_2 saturation vapor pressure at the corresponding temperature, except at 190 K. This implies that the rate of aggregation (R4) is not predominant relative to the rate of adsorption, i.e., $k_3 f < k_2(1-f)$, and then $k_2(1-f) + k_3 f \approx k_2(1-f)$ in Eq. (5). Furthermore, with low $P_{H_2O_2}$ and the short H_2O_2 exposure time (~ minute), we can assume that the surface coverage is low, $\theta \sim 0.1$, and approximately constant; then we have $f < 1$, and f can be

ACPD
11, 30091–30124, 2011

approximately treated as a constant. Equation (5) can be rewritten as:

$$\gamma_t \approx \frac{4Vk_1}{\omega S}\frac{k_2(1-f)}{k_{-1}+k_2(1-f)} \approx \frac{4Vk_1}{\omega S}\frac{1}{1+\frac{\nu_{-1}}{\nu_2}e^{(f-\frac{\Delta E}{RT})}} \quad (9)$$

where $\Delta E = E_{-1} - E_2$ and R is the gas constant. E_{-1} and E_2 are the activation energy of H_2O_2 from the precursor state to the gas phase and to the adsorption state, respectively. Equation (9) was used to fit the data in Fig. 4. $\Delta E = 28.5 \pm 7.0\,\mathrm{kJ\,mol^{-1}}$ was obtained from the least-squares fit. The activation energy of the uptake, $E_a = -\Delta E = -28.5 \pm 7.0\,\mathrm{kJ\,mol^{-1}}$, indicates that a precursor H_2O_2 molecule can easily overcome the barrier and traps in the adsorption state. It is a nonactivated adsorption process. E_a of H_2O_2 on the aqueous surface was determined to be $-26 \pm 7\,\mathrm{kJ\,mol^{-1}}$ (Worsnop et al., 1989), which is close to E_a of H_2O_2 on the ice surface, suggesting that the fitted $\Delta E = 28.5 \pm 7\,\mathrm{kJ\,mol^{-1}}$ is reasonable. The analysis from Eq. (9) also suggests that more H_2O_2 molecules are adsorbed on the ice surface at a lower temperature, i.e., 190 K. At a higher temperature, i.e., 220 K, we anticipate that the desorption of precursor H_2O_2 molecules to the gas phase has a higher probability than the migration of H_2O_2 to adsorption sites, and results in lower γ_t values.

4.2 Temperature programmed desorption

Panel (a) in Fig. 6 shows that H_2O_2 T_d of the first desorption peak of each desorption profile increases with an increase in H_2O_2 exposure, consistent with the zero-order desorption kinetics. Assuming that the zero-order kinetic formalism applies to the TPD data, the leading edge of the desorption profiles of the first peak in Panel (a) of Fig. 6 can be described using (Brown et al., 1996):

$$\text{Desorption rate} = \nu_0 e^{\frac{-E_d}{RT}} \quad (10)$$

where ν_0 is a pre-exponential factor and E_d is the desorption barrier. The long dashed line plotted in Panel (a) shows that the H_2O_2 desorption profile of the first desorption peak, at various exposures, can be perfectly described using Eq. (10), with

ACPD
11, 30091–30124, 2011

$v_0 = (1.0 \pm 0.3) \times 10^{26}$ molecules cm^{-3} s^{-1} and $E_d = 58.3 \pm 5.0$ kJ mol^{-1}. The excellent fit to the zero-order desorption kinetics suggests that H_2O_2 is multilayer adsorbed or islanded on the ice-film surface due to the lateral attractive interaction. Multilayer adsorption is expected because the exposure of H_2O_2 on the ice surface is high in TPD experiments. For example, for the lowest exposure (5-min H_2O_2 exposure) at 190 K, the amount of H_2O_2 taken up by the ice surface is 1.4×10^{15} molecules cm^{-2}, which is higher than a monolayer coverage of 2.7×10^{14} molecules cm^{-2}, estimated using the van der Waals radii of H_2O_2 3.42 Å (Huheey, 1983). The multilayer adsorption supports our previous assumption of the H_2O_2 molecule can be aggregated on ice surfaces for the analysis of the uptake coefficient data.

T_d of the H_2O_2 desorption peak centered at 225.0 K is identical to the T_d of ice, suggesting that H_2O_2 desorption at 225.0 K is accompanied by the ice desorption. Since H_2O_2 does not adsorb on the surface of the glass reactor wall (cf. Fig. 1), once H_2O desorption takes place, H_2O_2 desorbs along with ice. The nature of the H_2O_2 desorption peaks at 219.0 ± 0.5 K is not exactly clear to us. It may be due to H_2O_2 near distorted surface layers. The increase in T_d of ice from 225.0 K to 229.5 K, as the ice-film thickness increases from 14.3 µm to 36.0 µm, is attributed to the increased total lateral interactions among H_2O molecules for a thicker ice film (Yan and Chu, 2008).

5 Comparison and atmospheric implication

We may compare some of our findings with results from previous studies. Conklin et al. (1993) reported the sticking coefficient, α, to be 2.2×10^{-2} for H_2O_2 ($\sim 3 \times 10^{-5}$ Torr) loss on ~200-µm ice spheres at 228 K, from the analysis of the H_2O_2 breakthrough curves, using the advection-dispersion model. Our initial uptake coefficient γ_w is estimated to be $\sim 2 \times 10^{-3}$ at 228 K and 3×10^{-5} Torr. This γ_w value is lower than the α value. A possible explanation follows: since the α value was obtained from the overall forward rate constant of the advection-dispersion model, the model takes the adsorption of H_2O_2 on the surface, the distribution of H_2O_2 in the surface disor-

ACPD
11, 30091–30124, 2011

dered region and the diffusion of H_2O_2 into bulk ice into consideration, but the model does not separate these processes rigorously. With the long H_2O_2 exposure time to ice (up to 16 h) (Conklin et al., 1993), the transport of H_2O_2 to the near surface region and bulk cannot be ignored. In addition, co-condensation of H_2O with H_2O_2 also plays a role in the study of Conklin et al. (1993). The factors illustrated above cause a higher overall forward rate constant than the rate of the adsorption process alone. Our initial uptake coefficient measures the net H_2O_2 loss on the ice surface (cf. Eq. 4), since the H_2O_2 exposure time is short (~ minutes). This may explain the higher α value than our γ_w value. We also determined the amount of H_2O_2 taken up by ice surfaces (data are not shown). Our results show that the H_2O_2 uptake amount on ice films increases as temperature decreases, this is in agreement with the results of Conklin et al. (1993) and Pouvesle et al. (2010).

There is no reported γ value for H_2O_2 on ice surfaces at $T < 228$ K. The γ values of H_2O_2/ice may be compared to the γ values of atmospheric oxygenated organics on vapor deposited ice (Behr et al., 2006; Romanias et al., 2010). Table 3 shows γ values decrease gradually in an order from H_2O_2, CH_3COCH_3 to HCOOH. For these systems, the gas-surface interaction is mainly the van der Waals and hydrogen bonding interactions. The hydrogen bonding interaction for H_2O_2/ice is expected to be the strongest among the three systems, followed by HCOOH/ice and CH_3COCH_3/ice. Polarizability, $\bar{a}$, of the molecules decreases from CH_3COCH_3, HCOOH, to H_2O_2 (Table 3) (Schumb et al., 1955; Giguère, 1983; Lide, 2008), suggesting that the van der Waals interaction between CH_3COCH_3 and ice is the strongest, likely due to both C=O and CH_3 groups interact with the ice surface. The van der Waals interaction between H_2O_2 and ice is relatively weak, and H_2O_2/ice is dominated by the strong hydrogen bonding interaction. Cyclic HCOOH dimers in the gas phase via hydrogen bonds (Allouche, 2005) may affect the hydrogen bonding between HCOOH and ice. Along with low $\bar{a}$ for HCOOH, this may result in the low γ value listed in Table 3. Although the comparison is limited by the available data, it suggests that the interactions between H_2O_2 or oxygenated organics gases and ice involve both hydrogen bonds and van der Waals forces, and

ACPD
11, 30091–30124, 2011

the γ value depends on the nature of gas-surface interactions. The stronger the gas-surface interaction is, the higher the γ value is. For instance, the adsorption of H_2O_2 on TiO_2 surfaces is suggested to be a dissociative chemisorption (Pradhan et al., 2010), at room temperature, its room-temperature γ value is comparable with the γ values of other compounds listed in Table 3.

The activation energy of desorption for ice was determined to be $E_d = 48.0 \pm 3.0\,kJ\,mol^{-1}$ (Panel b, Fig. 6). This is in an excellent agreement with a value of $48.3 \pm 0.8\,kJ\,mol^{-1}$, reported by Brown et al. (1996). Since the binding energy ($26.4\,kJ\,mol^{-1}$) of the $H_2O_2{\cdot}H_2O_2$ dimer is higher than that of $H_2O{\cdot}H_2O$ dimer ($20.6\,kJ\,mol^{-1}$) (Schütz et al., 1997; Engdahl et al., 2001), using the similar analogy, we anticipate that the measured E_d of H_2O_2 ($58.3 \pm 5.0\,kJ\,mol^{-1}$) is higher than $E_d = 48\,kJ\,mol^{-1}$ of ice.

In order to assess the importance of the heterogeneous loss of H_2O_2 on ice/snow surfaces, we may compare heterogeneous lifetimes of H_2O_2 on cirrus clouds and on the snow/icepack (dry deposition) to a lifetime of H_2O_2 photolysis in the atmosphere. Cirrus clouds in the upper troposphere consist mainly of ice, and are surrounded by air. Using the first-order loss rate constant of $k_t = 1.4\,s^{-1}$ (calculated from $k_w = 55\,s^{-1}$, and corrected for ice porosity) for 8.9×10^{-6} Torr H_2O_2 on ice surfaces at 220 K and the typical S/V ratio of 10^{-3} ($cm^2\,cm^{-3}$) for a tropospheric cloud (Seinfeld and Pandis, 2006), the heterogeneous lifetime of H_2O_2 is estimated to be ~ 700 s. The atmospheric photolysis rate constant for H_2O_2 is $J = 1.2\times10^{-5}\,s^{-1}$ in the upper troposphere (Barth et al., 2007), and the photolysis lifetime of H_2O_2 is $1/J = 8.3\times10^4$ s. Thus, the heterogeneous loss of H_2O_2 on cirrus cloud surfaces is more efficient process than that of the H_2O_2 photolysis. On the ground-level snow/ice surfaces, the heterogeneous lifetime of H_2O_2 is estimated to be $\sim 4\times10^{-3}$ s using the S/V ratio ~ 200 ($cm^2\,cm^{-3}$) for the typical snow/ice surface (Dominé et al., 2002). This value is smaller than that of photolysis, 8.3×10^4 s, with an assumption that J of H_2O_2 at ground level is similar to that in the upper troposphere. However, dry deposition consists of aerodynamic and quasi-laminar

ACPD
11, 30091–30124, 2011

sublayer transports, and the heterogeneous uptake (Seinfeld and Pandis, 2006). The air parcel containing H_2O_2 needs to transport to the icepack surface. With a dry deposition velocity of H_2O_2 0.32 cm s^{-1} over the snow/ice surfaces, and the average travel length of ~10 m from the air to the snow/ice surface (Seinfeld and Pandis, 2006), the dry deposition time is estimated to be $\sim 3\times10^3$ s, which is orders of magnitude longer than the heterogeneous lifetime of H_2O_2, 4×10^{-3}, on ice, suggesting that the heterogeneous loss of H_2O_2 on icepack at ground level is limited by the transport process (dry deposition), not by heterogeneous chemistry. The heterogeneous loss of H_2O_2 on snow/ice surfaces is faster than the gas-phase photolysis rate of H_2O_2. In summary, the loss of H_2O_2 to ice surfaces, such as cirrus clouds and snow/icepack, may be a sink for H_2O_2 at low temperature. However, at warmer temperature, our TPD results and other studies (Clegg and Abbatt, 2001) suggest that ice is not a permanent sink for H_2O_2.

6 Conclusions

We have determined the initial uptake coefficient of H_2O_2 on ice surfaces using the flow reactor. γ_t of H_2O_2 increases from 1.3×10^{-3} to 8.8×10^{-3} on ice films, as the H_2O_2 partial pressure increases from 7.9×10^{-6} to 4.7×10^{-5} Torr at 190 K. The γ_t value of H_2O_2 decreases from 1.2×10^{-3} to 6.6×10^{-5} as the temperature increases from 190 to 220 K. Uptake of H_2O_2 on ice involves both adsorption and aggregation of H_2O_2 on the ice surfaces. The study suggests that the nature of H_2O_2-ice surface interactions is mainly hydrogen bonds. The results imply that gaseous H_2O_2 can be taken up by snow/ice or icepack, with $\gamma_w \leq 0.1$ at low temperatures, and our results are useful to model the H_2O_2 loss on snow/ice and cirrus clouds.

Acknowledgements. The authors would like to thank Terence Wagenknecht for the loan of a Bausch & Lomb refractometer. This work was supported in part by the National Science Foundation under grant ATM-0355521.

ACPD
11, 30091–30124, 2011

References

Allouche, A.: Quantum studies of hydrogen bonding in formic acid and water ice surface, J. Chem. Phys., 122, 234703, doi:10.1063/1.1929733, 2005.

Bales, R. C., Losleben, M. V., McConnell, J. R., Fuhrer, K., and Neftel, A.: H_2O_2 in snow, air and open pore space in firn at Summit, Greenland, Geophys. Res. Lett., 22, 1261–1264, 1995.

Barth, M. C., Kim, S.-W., Skamarock, W. C., Stuart, A. L., Pickering, K. E., and Ott, L. E.: Simulations of the redistribution of formaldehyde, formic acid, and peroxides in the 10 July 1996 Stratospheric-Tropospheric experiment: radiation, aerosols, and ozone deep convection storm, J. Geophys. Res., 112, D13310, doi:10.1029/2006JD008046, 2007.

Behr, P., Terziyski, A., and Zellner, R.: Acetone adsorption on ice surfaces in the temperature range $T = 190$–220 K: evidence for aging effects due to crystallographic changes of the adsorption sites, J. Phys. Chem. A, 110, 8098–8107, 2006.

Bowker, M. and King, D. A.: Anomalous adsorption kinetics. γ-Nitrogen on the {110} plane of tungsten, J. Chem. Soc. Faraday Trans. I, 75, 2100–2115, 1979.

Brown, R. L.: Tubular flow reactors with first-order kinetics, J. Res. Nat. Bur. Stand., 83, 1–8, 1978.

Brown, D. E., George, S. M., Huang, C., Wong, E. K. L., Rider, K. B., Smith, R. S., and Bruce, D. K.: H_2O condensation coefficient and refractive index for vapor-deposited ice from molecular beam and optical interference measurements, J. Phys. Chem., 100, 4988–4995, 1996.

Chu, L. and Anastasio, C.: Formation of hydroxyl radical from the photolysis of frozen hydrogen peroxide, J. Phys. Chem. A, 109, 6264–6271, 2005.

Chu, L. and Chu, L. T.: Heterogeneous reaction $HOCl + HBr \rightarrow BrCl + H_2O$ on ice films, J. Phys. Chem. A, 103, 691–699, 1999.

Chu, L. T. and Heron, J. W.: Uptake of HBr on ice at polar atmospheric conditions, Geophys. Res. Lett., 22, 3211–3214, 1995.

Chu, L. T., Leu, M.-T., and Keyser, L. F.: Heterogeneous reactions of $HOCl + HCl \rightarrow Cl_2 + H_2O$ and $ClONO_2 + HCl \rightarrow Cl_2 + HNO_3$ on ice surfaces at polar stratospheric conditions, J. Phys. Chem., 97, 12798–12804, 1993.

Clegg, S. M. and Abbatt, J. P. D.: Uptake of gas-phase SO_2 and H_2O_2 by ice surfaces: dependence on partial pressure, temperature, and surface acidity, J. Phys. Chem. A, 105,

ACPD
11, 30091–30124, 2011

6630–6636, 2001.
Conklin, M. H., Sigg, A., Neftel, A., and Bales., R. C.: Atmosphere-snow transfer function for H_2O_2: microphysical considerations, J. Geophys. Res., 98, 18367–18376, 1993.
Cussler, E. L.: Diffusion, mass transfer in fluid systems, Cambridge University Press, NY, 1984.
Davis, E. J.: Interpretation of uptake coefficient data obtained with flow tubes, J. Phys. Chem. A, 112, 1922–1932, 2008.
Dean, J. A.: Lange's Handbook of Chemistry, 15th edn., McGraw-Hill, NY, Sec. 6.129, 1999.
Dominé, F. Cabanes, A., and Legagneux, L.: Structure, microphysics, and surface area of the Arctic snowpack near Alert during the ALERT 2000 campaign, Atmos. Environ., 36, 2753–2765, 2002.
Engdahl, A., Nelander, B., and Karlström, G.: A matrix isolation and ab initio study of the hydrogen peroxide dimer, J. Phys. Chem. A, 105, 8393–8398, 2001.
France, J. L., King, M. D., and Lee-Taylor, J.: Hydroxyl (OH) radical production rates in snowpacks from photolysis of hydrogen peroxide (H_2O_2) and nitrate (NO_3^-), Atmos. Environ., 41, 5502–5509, 2007.
Giguère, P. A.: Molecular association and structure of hydrogen peroxide, J. Chem. Educ., 60, 399–401, 1983.
Giguère, P. A. and Geoffrion, P.: Refractive index of hydrogen peroxide solutions. A revision, Can. J. Res. B, 27, 168–173, 1949.
Giguère, P. A. and Maass, O.: Solid solutions of hydrogen peroxide and water, Can. J. Res. B, 18, 66–73, 1940.
Grannas, A. M., Jones, A. E., Dibb, J., Ammann, M., Anastasio, C., Beine, H. J., Bergin, M., Bottenheim, J., Boxe, C. S., Carver, G., Chen, G., Crawford, J. H., Dominé, F., Frey, M. M., Guzmán, M. I., Heard, D. E., Helmig, D., Hoffmann, M. R., Honrath, R. E., Huey, L. G., Hutterli, M., Jacobi, H. W., Klán, P., Lefer, B., McConnell, J., Plane, J., Sander, R., Savarino, J., Shepson, P. B., Simpson, W. R., Sodeau, J. R., von Glasow, R., Weller, R., Wolff, E. W., and Zhu, T.: An overview of snow photochemistry: evidence, mechanisms and impacts, Atmos. Chem. Phys., 7, 4329–4373, doi:10.5194/acp-7-4329-2007, 2007.
Huckaba, C. E. and Keyes, F. G.: The density of aqueous hydrogen peroxide solutions, J. Am. Chem. Soc., 70, 2578–2581, 1948.
Huheey, J. E.: Inorganic chemistry, 3rd edn., Harper & Row, NY, Chapter 6, 1983.
Hutterli, M. A., McConnell, J. R., Stewart, R. W., Jacobi, H.-W., and Bales, R. C.: Impact of temperature-driven cycling of hydrogen peroxide (H_2O_2) between air and snow on the

ACPD
11, 30091–30124, 2011

planetary boundary layer, J. Geophys. Res., 106, 15395–15404, 2001.
Jacobi, H.-W., Annor, T., and Quansah, E.: Investigation of the photochemical decomposition of nitrate, hydrogen peroxide, and formaldehyde in artificial snow, J. Photoch. Photobio. A, 179, 330–338, 2006.
Jin, R. and Chu, L. T.: Uptake of NH_3 and NH_3 + HOBr reaction on ice surfaces at 190 K, J. Phys. Chem. A, 111, 7833–7840, 2007.
Kahan, T. F., Zhao, R., and Donaldson, D. J.: Hydroxyl radical reactivity at the air-ice interface, Atmos. Chem. Phys., 10, 843–854, doi:10.5194/acp-10-843-2010, 2010.
Keyser, L. F. and Leu, M.-T.: Surface areas and porosities of ices used to simulate stratospheric clouds, J. Colloid Interf. Sci., 155, 137–145, 1993a.
Keyser, L. F. and Leu, M.-T.: Morphology of nitric acid and water ice films, Microsc. Res. Techniq., 25, 434–438, 1993b.
Keyser, L. F., Moore, S. B., and Leu, M.-T.: Surface reaction and pore diffusion in flow-tube reactors, J. Phys. Chem., 95, 5496–5502, 1991.
Keyser, L. F., Leu, M.-T., and Moore, S. B.: Comment on porosities of ice films used to simulate stratospheric cloud surfaces, J. Phys. Chem., 97, 2800–2801, 1993.
Kulkarni, A. D., Pathak, R. K., and Bartolotti, L. J.: Effect of additional hydrogen peroxide to $H_2O_2 \ldots (H_2O)_n$, n = 1 and 2 complexes: quantum chemical study, J. Chem. Phys., 124, 214309, doi:10.1063/1.2202098, 2006.
Lide, D. R. (ed.): CRC Handbook of Chemistry and Physics, 88th edn., CRC Press, Boca Raton, FL, 2008.
Maass, O. and Hatcher, W. H.: The properties of pure hydrogen peroxide. I., J. Am. Chem. Soc., 42, 2548–2569, 1920.
Manatt, S. L. and Manatt, M. R. R.: On the analyses of mixture vapor pressure data: the hydrogen peroxide/water system and its excess thermodynamic functions, Chem. Eur. J., 10, 6540–6557, 2004.
Masel, R. I.: Principles of adsorption and reaction on solid surfaces, Wiley, NY, 1996.
Motz, H. and Wise, H.: Diffusion and heterogeneous reaction. III. Atom recombination at a catalytic boundary, J. Chem. Phys., 32, 1893–1894, 1960.
Panczyk, T., Fiorin, V., Blanco-Alemany, R., and King, D. A.: Dynamics of water adsorption on Pt{110}-(1×2): a molecular dynamics study, J. Chem. Phys., 131, 064703, doi:10.1063/1.3204700, 2009
Pouvesle, N., Kippenberger, M., Schuster G., and Crowley, J. N.: The interaction of H_2O_2 with

ACPD
11, 30091–30124, 2011

ice surfaces between 203 and 233 K, Phys. Chem. Chem. Phys., 12, 15544–15550, 2010.
Pradhan, M., Kalberer, M., Griffiths, P. T., Braban, C. F., Pope, F. D., Cox, R. A., and Lambert, R. M.: Uptake of gaseous hydrogen peroxide by submicrometer titanium dioxide aerosol as a function of relative humidity, Environ. Sci. Technol., 44, 1360–1365, 2010.
Romanias, M. N., Zogka, A. G., Stefanopoulos, V. G., Papadimitriou, V. C., and Papagiannakopoulos, P.: Uptake of formic acid on thin ice films and on ice doped with nitric acid between 195 and 211 K, Chem. Phys. Chem., 11, 4042–4052, 2010.
Satterfield, C. N.: Mass transfer in heterogeneous catalysis, MIT, Cambridge, Chapter 3, 1970.
Scatchard, G., Kavanagh, G. M., and Ticknor, L. B.: Vapor-liquid equilibrium. VIII. Hydrogen peroxide-water mixtures, J. Am. Chem. Soc., 74, 3715–3720, 1952.
Schumb, W. C., Satterfield, C. N., and Wentworth, R. L.: Hydrogen peroxide, ACS Monograph Series, Reinhold Publishing Corp., NY, Chapter 5, 1955.
Schütz, M., Brdarski, S., Widmark, P. O., Lindh, R., and Karlström, G.: The water dimer interaction energy: convergence to the basis set limit at the correlated level, J. Chem. Phys., 107, 4597–4605, 1997.
Seinfeld, J. H. and Pandis, S. N.: Atmospheric chemistry and physics, 2nd edn., Wiley, Hoboken, NJ, 2006.
Sigg, A. and Neftel, A.: Evidence for a 50 % increase in H_2O_2 over the past 200 years from a Greenland ice core, Nature, 351, 557–559, 1991.
Vione, D., Maurino, V., Minero, C., and Pelizzetti, E.: The atmospheric chemistry of hydrogen peroxide: a review, Ann. Chim.-Rome, 93, 477–488, 2003.
Worsnop, D. R., Zahniser, M. S., Kolb, C. E., Gardner, J. A., Watson, L. R., Van Doren, J. M., Jayne, J. T., and Davidovits, P.: Temperature dependence of mass accommodation of SO_2 and H_2O_2 on aqueous surfaces, J. Phys. Chem., 93, 1159–1172, 1989.
Yan, H. and Chu, L. T.: Interactions of oxalic acid and ice on Cu surface, Langmuir, 24, 9410–9420, 2008.
Yan, H., Chu, L. T., Jin, R., and Diao, G.: Studies of atmospherically relevant reactions using differentially pumped mass spectrometer and Fourier transform infrared spectroscopy, Spectrosc. Lett., 42, 444–457, 2009.

ACPD
11, 30091–30124, 2011

Table 1. Uptake coefficients for H_2O_2 on ice surfaces at 190 K[a].

$P_{H_2O_2}$ (Torr)	T (K)	v[b] ($m\,s^{-1}$)	k_s (s^{-1})	k_w (s^{-1})	γ_w	γ_t[c]
$(7.9 \pm 0.6) \times 10^{-6}$	189.9 ± 0.3	18.8	250 ± 31	280 ± 36	$(1.4 \pm 0.2) \times 10^{-2}$	$(1.3 \pm 0.3) \times 10^{-3}$
$(1.2 \pm 0.1) \times 10^{-5}$	189.8 ± 0.3	19.0	316 ± 38	366 ± 96	$(1.9 \pm 0.5) \times 10^{-2}$	$(2.0 \pm 0.8) \times 10^{-3}$
$(1.5 \pm 0.1) \times 10^{-5}$	190.1 ± 0.3	19.1	444 ± 54	547 ± 71	$(2.8 \pm 0.4) \times 10^{-2}$	$(3.9 \pm 0.8) \times 10^{-3}$
$(2.0 \pm 0.1) \times 10^{-5}$	190.0 ± 0.2	19.0	456 ± 62	567 ± 82	$(2.9 \pm 0.4) \times 10^{-2}$	$(4.1 \pm 1.0) \times 10^{-3}$
$(2.2 \pm 0.1) \times 10^{-5}$	190.1 ± 0.3	18.6	495 ± 97	630 ± 138	$(3.2 \pm 0.7) \times 10^{-2}$	$(4.8 \pm 1.6) \times 10^{-3}$
$(2.9 \pm 0.1) \times 10^{-5}$	190.2 ± 0.2	18.8	565 ± 88	744 ± 131	$(3.7 \pm 0.6) \times 10^{-2}$	$(6.3 \pm 1.8) \times 10^{-3}$
$(3.7 \pm 0.1) \times 10^{-5}$	189.9 ± 0.4	18.6	613 ± 70	830 ± 102	$(4.2 \pm 0.5) \times 10^{-2}$	$(7.4 \pm 1.4) \times 10^{-3}$
$(4.7 \pm 0.1) \times 10^{-5}$	189.8 ± 0.2	19.0	676 ± 94	941 ± 147	$(4.7 \pm 0.7) \times 10^{-2}$	$(8.8 \pm 2.0) \times 10^{-3}$

[a] The ice-film thickness was 14.7 ± 1.5 µm.
[b] Flow velocity.
[c] γ_t was calculated from Eq. (3) using $N_L = 13$ at $h = 14.7$ µm.

ACPD
11, 30091–30124, 2011

Table 2. Uptake coefficients for H_2O_2 on ice surfaces at varying temperature[a].

T (K)	v^b ($m\,s^{-1}$)	k_s (s^{-1})	k_w (s^{-1})	γ_w	γ_t^c
189.8 ± 0.2	19.3	241.4 ± 52.8	269.2 ± 61.8	$(1.4 \pm 0.3) \times 10^{-2}$	$(1.2 \pm 0.5) \times 10^{-3}$
194.6 ± 0.2	18.9	226.1 ± 34.4	250.2 ± 39.3	$(1.3 \pm 0.2) \times 10^{-2}$	$(1.1 \pm 0.4) \times 10^{-3}$
200.0 ± 0.2	19.4	162.4 ± 38.2	174.5 ± 46.9	$(8.7 \pm 2.0) \times 10^{-3}$	$(5.4 \pm 2.5) \times 10^{-4}$
204.7 ± 0.3	20.1	116.9 ± 51.8	123.1 ± 56.3	$(6.1 \pm 2.7) \times 10^{-3}$	$(2.8 \pm 1.3) \times 10^{-4}$
209.7 ± 0.3	20.9	109.3 ± 14.2	114.6 ± 14.9	$(5.6 \pm 0.7) \times 10^{-3}$	$(2.5 \pm 1.1) \times 10^{-4}$
214.2 ± 0.3	21.3	82.2 ± 24.8	85.2 ± 26.1	$(4.1 \pm 1.2) \times 10^{-3}$	$(1.4 \pm 0.7) \times 10^{-4}$
219.1 ± 0.2	22.0	53.7 ± 13.4	54.8 ± 13.5	$(2.6 \pm 0.6) \times 10^{-3}$	$(6.6 \pm 2.8) \times 10^{-5}$

[a] $P_{H_2O_2} = (8.9 \pm 0.4) \times 10^{-6}$ Torr, and the thickness of ice films was 36.1 ± 1.8 µm.
[b] Flow velocity.
[c] γ_t was calculated from Eq. (3) using $N_L = 17$ at $h = 36.1$ µm.

ACPD
11, 30091–30124, 2011

Table 3. Comparison of uptake coefficients on vapor deposited ice.

	$10^3\gamma$[a]	Surface	Reference	$\bar{a}$ (10^{-24} cm^3)
H_2O_2	8.7	ice	This work	2.3
CH_3COCH_3	6	ice	Behr et al. (2006)	6.3
HCOOH	2	ice	Romanias et al. (2010)	3.4
H_2O_2	1.5[b]	TiO_2	Pradhan et al. (2010)	

[a] At 8.9×10^{-6} Torr and 199.0 ± 1.0 K.
[b] At 1.3×10^{-4} Torr, 295 K and 15 % relative humidity.

ACPD
11, 30091–30124, 2011

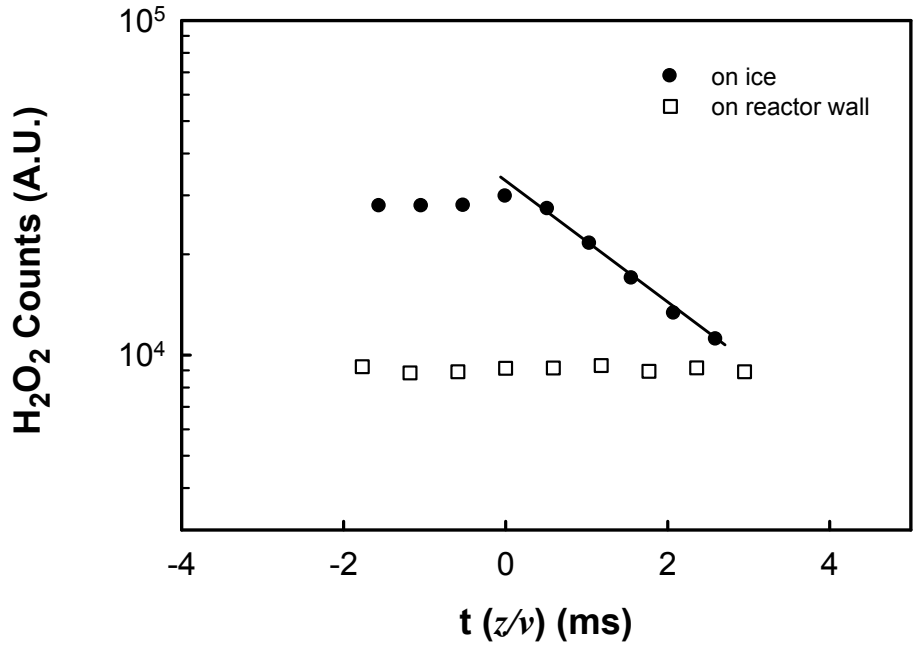

Fig. 1. Plot of the log H_2O_2 signal versus contact time ($t = z/v$) at 190 K. The plot shows the initial H_2O_2 signal, before H_2O_2 came in contact with the ice ($t < 0$), and the loss of H_2O_2 onto the ice film ($t > 0$). The background H_2O_2 signal was subtracted. The first-order loss rate constant for H_2O_2 on ice was determined to be $k_s = 444 \pm 13\,s^{-1}$, and the corrected rate constant $k_w = 549 \pm 19\,s^{-1}$, and $\gamma_w = 2.8 \times 10^2$. The ice-film thickness was 13.8 µm, and $P_{H_2O_2} = 1.5 \times 10^{-5}$ Torr. The loss of H_2O_2 signal onto the reactor wall shows that there is no H_2O_2 loss to the cold glass reactor wall, $P_{H_2O_2} = 1.0 \times 10^{-5}$ Torr. Data were offset for clarity.

ACPD
11, 30091–30124, 2011

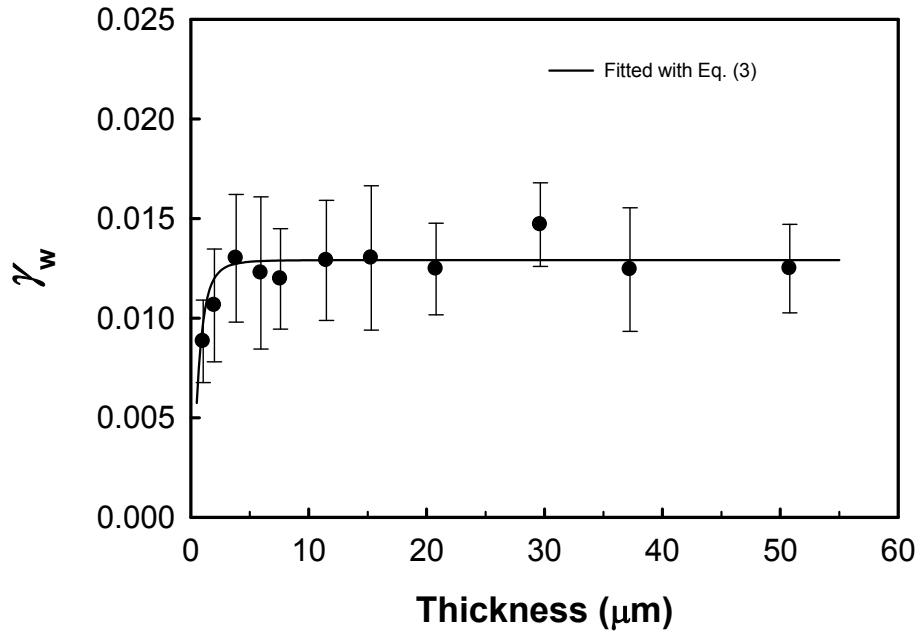

Fig. 2. Plot of the initial uptake coefficient of H_2O_2, γ_w, on ice as a function of the ice-film thickness at 190.0 ± 0.2 K. Fitted parameters are $a = -0.35$, $b = 11.03$ and $c = 1.002$. $P_{H_2O_2} = (8.2 \pm 0.3) \times 10^{-6}$ Torr, and the γ_t value was determined to be $(1.1 \pm 0.2) \times 10^{-3}$ (see text).

ACPD
11, 30091–30124, 2011

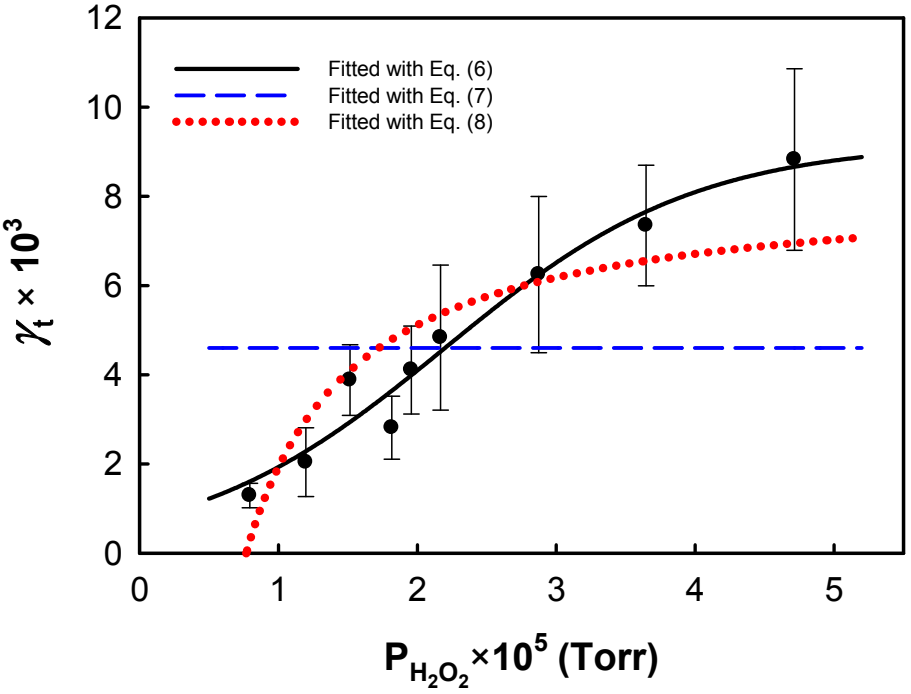

Fig. 3. Plot of the true uptake coefficient of H_2O_2, γ_t, on the ice surface versus H_2O_2 partial pressure at 190 K. The ice-film thickness was 14.7 ± 1.5 µm. See text for details.

ACPD
11, 30091–30124, 2011

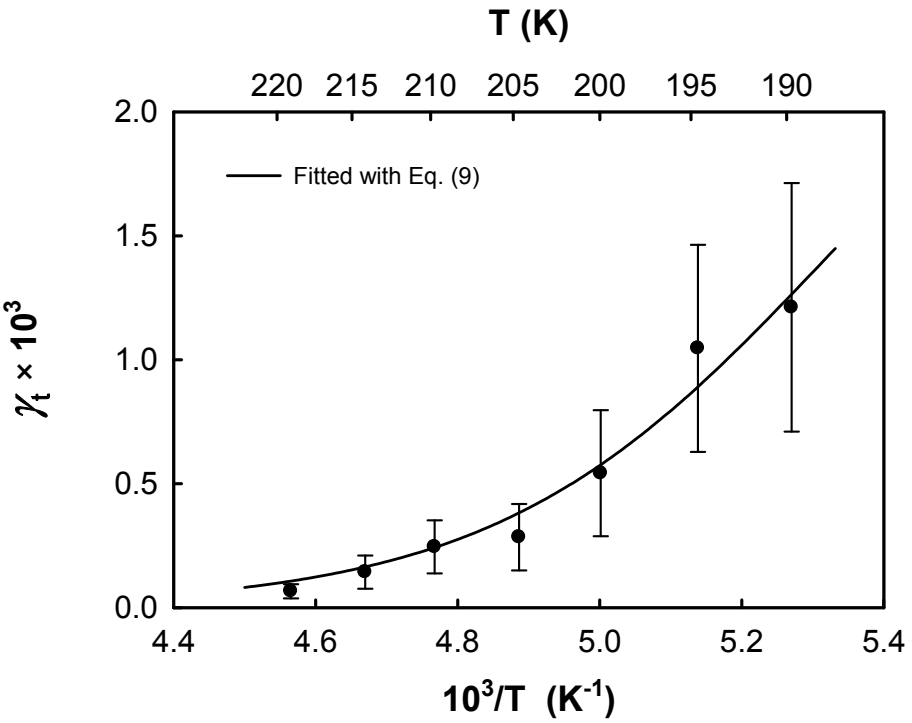

Fig. 4. Plot of the true uptake coefficient of H_2O_2, γ_t, on the ice surface versus $1/T$. $P_{H_2O_2}$ = $(8.9 \pm 0.4) \times 10^{-6}$ Torr.

ACPD
11, 30091–30124, 2011

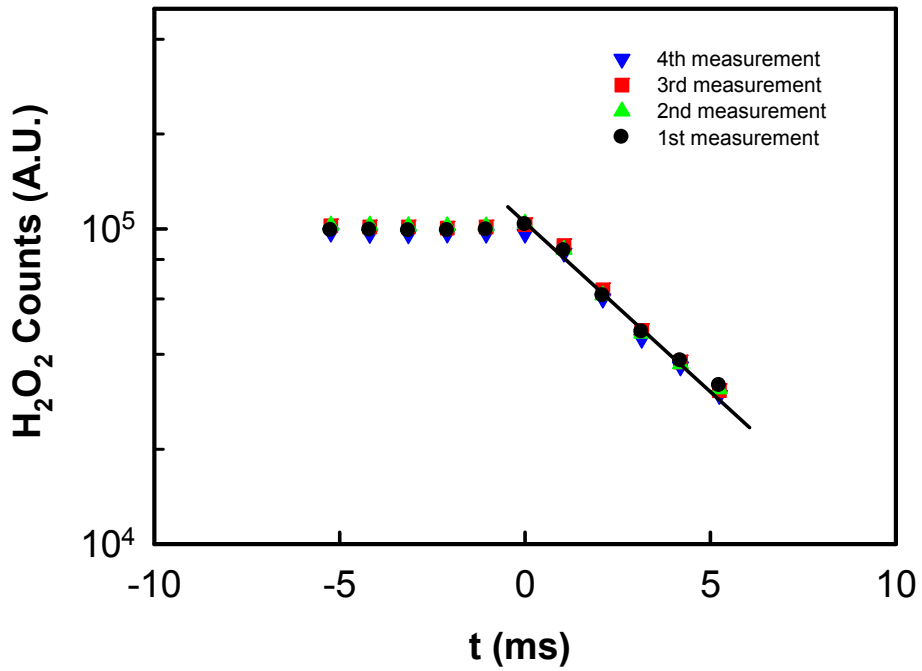

Fig. 5. Plot of the H_2O_2 signal versus the gas-surface contact time for four repeated measurements on an ice film at 190.0 K. The initial uptake coefficient, γ_w, calculated from the slopes of the data using the least-squares fit to Eq. (1) (solid line), to be 1.8×10^{-2}. After the first measurement, the injector was then pushed back to the downstream end to enable subsequent measurements to be made on the same ice film. The background H_2O_2 signal has been subtracted from the plotted values. The thickness of the ice film was 14.7 µm, and the total pressure was 0.500 Torr. See text for details.

ACPD
11, 30091–30124, 2011

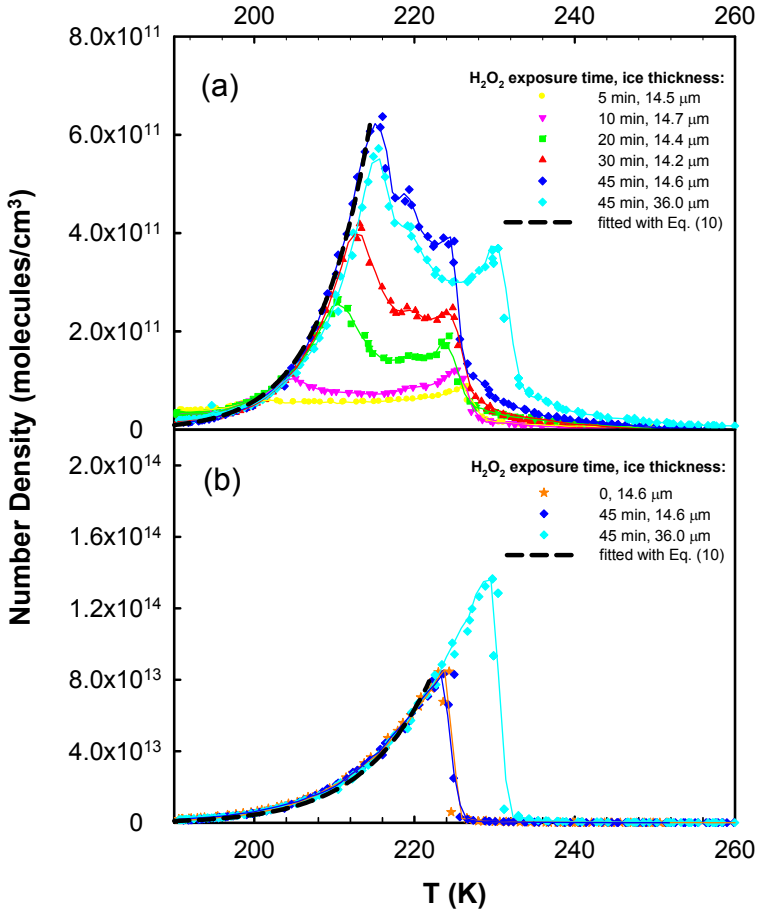

Fig. 6. TPD of H_2O_2 on ice films. **(a)** H_2O_2 TPD profiles, **(b)** H_2O TPD profiles. Ice films were exposed to gaseous H_2O_2 at 190 K and $P_{H_2O_2} = (2.2 \pm 0.1) \times 10^{-5}$ Torr.

ACPD
11, 30091–30124, 2011

Uptake coefficient of H_2O_2 on ice

H. Yan and L. T. Chu